Temperature-dependent frictional properties of ultra-thin boron nitride nanosheets

Wenyang Qu, Xiaoming Chen, and Changhong Ke

Citation: Appl. Phys. Lett. **110**, 143110 (2017); doi: 10.1063/1.4979835
View online: http://dx.doi.org/10.1063/1.4979835
View Table of Contents: http://aip.scitation.org/toc/apl/110/14
Published by the American Institute of Physics

Temperature-dependent frictional properties of ultra-thin boron nitride nanosheets

Wenyang Qu,[1] Xiaoming Chen,[1] and Changhong Ke[1,2,a)]
[1]*Department of Mechanical Engineering, State University of New York at Binghamton, Binghamton, New York 13902, USA*
[2]*Materials Science and Engineering Program, State University of New York at Binghamton, Binghamton, New York 13902, USA*

(Received 13 February 2017; accepted 22 March 2017; published online 5 April 2017)

We investigate the temperature-dependent frictional properties of mono- and few-layer hexagonal boron nitride nanosheets (BNNSs) by using atomic force microscopy (AFM). The measurements reveal that a modest increase in sample temperature results in a substantial decrease of the frictional force between a silicon AFM tip and a BNNS, and the frictional force change is modulated by the scan velocity of the AFM tip and the number of layers in the BNNS. The activation energy of the contact rupture for the examined BNNSs is found to be around 0.35 eV, which is substantially higher than the reported values for graphene. The observed high activation energy for the BNNS is ascribed to its electronically and topographically corrugated surface, which originates from the polarized nature of B-N bonds and the size difference of B and N atoms. The findings are useful to better understand the physical properties of hexagonal BNNS materials and in the pursuit of their applications, such as substrate materials in nano electronic devices. *Published by AIP Publishing*. [http://dx.doi.org/10.1063/1.4979835]

Hexagonal boron nitride nanosheets (BNNSs), the so-called white graphene, possess superior mechanical[1,2] and thermal conducting[3] properties and thermal and chemical stabilities.[4] As a semiconductor with a reported bandgap of nearly 6 eV,[5] BNNSs are electrically insulating in nature, which enables their applications in optoelectronics and as dielectric substrate materials for high-performance graphene nanoelectronics.[6] It is reported that the mobility of graphene devices on BNNS substrates is of one order of magnitude higher than that achieved on silicon oxide substrates. In addition to the advantages of small surface roughness and small lattice mismatch with graphene, BNNS substrates in graphene electronics dissipate a majority of heat, which is produced by electrical current, through a reportedly ballistic thermal transport phenomenon on the graphene-BN interface. Temperature-dependent frictional properties of BNNSs are expected to play an important role in their applications. This is because thermal activation helps enable the relative sliding through overcoming the local energy barriers in the energy landscape of two bodies in contact.[7,8] The resulting lateral sliding and/or the normal spacing variation between layered-stacked graphene-BNNSs may have a substantial impact on the electron and phonon transport and thus the overall device properties, performance, and reliability. Even though there are a number of reported studies on the temperature-dependent frictional properties of graphene or graphite,[9–11] the same properties of BNNSs remain largely unexplored. From a structural point of view, hexagonal BN (h-BN) sheets are made of partially ionic B-N bonds and possess topographically and electronically corrugated surfaces. The frictional properties of BNNSs are likely governed by thermodynamic processes that are far more rich and complex as compared with those of graphene. It is noted that individual hopping events on a corrugated energy landscape[8] can be well described using the so-called "stick-slip" model.[12–14] The stick-slip model has been widely used to analyze frictional measurements and study the friction properties at the small scale[15] and is thus an important theoretical tool in studying the frictional properties of BNNSs.

In this paper, we investigate the temperature-dependent frictional properties of mono- and few-layer BNNSs by using atomic force microscopy (AFM). The measurements reveal that a modest increase in sample temperature results in a substantial decrease of the frictional force between an AFM tip and a BNNS, and the frictional force change is modulated by the scan velocity of the AFM tip and the number of layers in the BNNS. The activation energy of the contact rupture for the examined BNNS is found to be around 0.35 eV and is substantially higher than the reported values (~0.1 eV) for graphene. The findings indicate that the topographically and electronically corrugated h-BN surfaces possess a substantially higher energy barrier to contacting bodies than the otherwise smooth and electrically neutral surface of graphene.

The employed BNNSs in this study were prepared by means of mechanically exfoliating commercially available hexagonal BN powders (Momentive, PT110).[16] After being transferred to silicon oxide substrates, BNNS flakes were examined by using optical/Raman microscopy and AFM. Mono- and few-layer BNNSs were identified and subsequently characterized in the AFM-based frictional measurements, which are illustrated in Figure 1(a). All of the AFM measurements presented in this paper were performed inside a Park Systems XE-70 AFM with closed-loop piezo stages, which was housed inside an environmental chamber with a computerized humidity control. A computer-controlled thermoelectric

a)Author to whom correspondence should be addressed. Electronic mail: cke@binghamton.edu

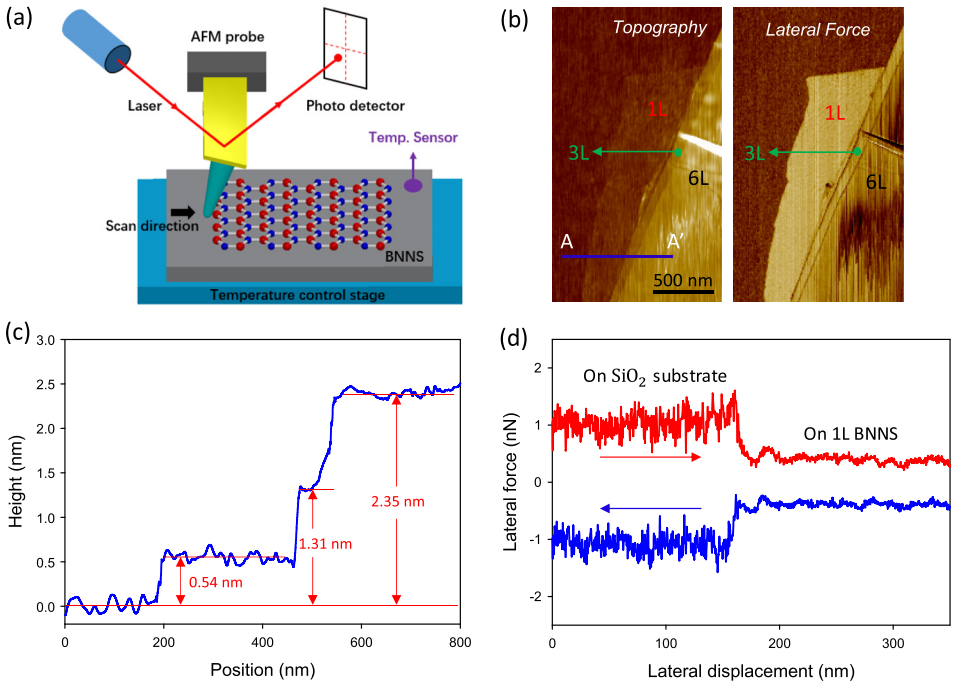

FIG. 1. (a) Schematic of BNNS frictional measurements by using lateral atomic force microscopy (AFM) techniques. (b) AFM topography (*left*) and lateral force (*right*) images of one BNNS flake that is composed of 1L, 3L, and 6L BNNS regions. (c) AFM height profile of the BNNS shown in (b) along the marked blue line. (d) The frictional loop measured on the 1L BNNS shown in (b) along the marked blue line. The arrows indicate the AFM tip scan directions.

heating/cooling stage, which was placed underneath the silicon oxide substrate with BNNS flakes that stay on top, was employed to control the sample temperature for the frictional and adhesion measurements. Frictional and adhesion measurements were carried out at a humidity of 10%, and at four sample temperatures within 293–313 K, each of which was measured as the temperature of the top surface of the substrate adjacent to the BNNS samples. Silicon nitride AFM cantilevers with silicon tips (model CSG 10, NT-MDT) were employed for all frictional/adhesion measurements. The spring constant of each employed AFM cantilever was calibrated using thermal tuning methods[17] at each testing temperature and was found to be within the range of 0.18–0.46 N/m. The lateral sensitivity of each cantilever was calibrated by following a two-slope wedge method using a TGG01 silicon grating[18] and was found to be within the range of 22.6–46.8 nN/V. The tip radii of the AFM probes were estimated to be 10–20 nm by following a previously reported approach.[17] For frictional measurements, the AFM was operated in a lateral force mode with AFM tip scan rates within the range of 250–2000 nm/s and applied normal compressive loads of 0.05–4 nN.

Figure 1(b) shows the AFM topography and the corresponding lateral force images of one BNNS flake on the surface of a silicon oxide substrate. Its topography profile along the marked A-A' section is exhibited in Figure 1(c), which displays three steps with heights of about 0.54, 1.31, and 2.35 nm, respectively. By considering an interlayer distance of 0.34 nm in the BNNS and correlating the measured sheet heights with the corresponding Raman profiles as displayed in Figure S1 (supplementary material), it is concluded that this flake is composed of one-layer (1L), 3L, and 6L BNNS domains. Raman spectra of BNNS flakes of 1L, 2L, 3L, 6L, and 9L domains were characterized in this study. It is noted that the G band (E_{2g} mode) peak location/full width at half maximum (FWHM) of 1L and 3L BNNSs are measured to be 1369.2/16.8 cm^{-1} and 1367.8/10.2 cm^{-1}, respectively, all of which are consistent with prior data in the literature.[4] Both the G band peak and FWHM of the examined BNNSs exhibit a decreasing trend with an increase in the number of layers. The values measured for 9L BNNS samples (1365.8/8.6 cm^{-1}) are close to the respective values reported for bulk h-BN (1366.2/9 cm^{-1}).[4,16,19] The surface roughnesses of the substrate and BNNSs are of importance to their frictional properties and are measured based on the recorded AFM topography images. Figure S2 (supplementary material) shows the surface roughness of the examined BNNS samples at various temperatures. The data show that the BNNS surface roughness decreases with its thickness and tends to plateau for thicker samples. The surface roughness of the employed silicon oxide substrate is found to slightly decrease with an increase in the sample temperature and to be within the range of about 0.19–0.23 nm (inset plot in Figure S2 of the supplementary material). The surface roughness of the 1L BNNS is close to that of the substrate, while much lower values are observed for 6L and 9L BNNSs. This observation is consistent with prior findings reported for graphene that the surface roughness of 2D nanosheets is governed by the substrate roughness as well as their bending stiffnesses.[20–23] The thicker BNNS possesses a higher bending rigidity that helps to resist the sample-substrate adhesion-induced deflection, resulting in a smaller surface roughness. It is also consistently displayed in Figure S2 (supplementary material) that an increasing sample temperature results in a noticeable decrease of the surface roughness for mono- and few-layer BNNSs. The adhesion force between the AFM probe and the BNNS samples was characterized by performing pull-off tests,[24] and the measured values are reported in Figure S3 (supplementary material). The data show that the sample thickness has little influence on the adhesion force, while an increasing sample temperature leads to a noticeable increase in the adhesion force. Figure 1(d)

shows an AFM frictional loop that was recorded in the 1L region along the marked A-A′ section in Figure 1(b). The measurement was performed at a sample temperature of 293 K with an applied compressive load of 0.05 nN and an AFM tip scan rate of 1000 nm/s. The frictional force on the surface of the 1L BNNS was measured to be 0.41 ± 0.05 nN, which is substantially lower compared to the value measured on the silicon oxide substrate (1.1 ± 0.15 nN).

Figure 2(a) shows the measured frictional force on the 1L BNNS surface as a function of the applied compressive load under the same scan rate of 1000 nm/s. The measured dependence of the friction force on the applied load can be well-fitted using a power function given as $f \sim (P + P_A)^{2/3}$,[24] where f is the friction force, P is the applied load, and P_A is the adhesion force between the AFM tip and the BNNS. Through curve fitting of the profiles shown in Figure 2(a), the value of P_A is obtained and displayed in Figure 2(b). It is found to be within the range of 3.7–4.1 nN and is 11%–20% higher than the respective values obtained from the pull-off measurements. The two plots of the adhesion force shown in Figure 2(b) display a similar increasing trend in its dependence on the sample temperature.

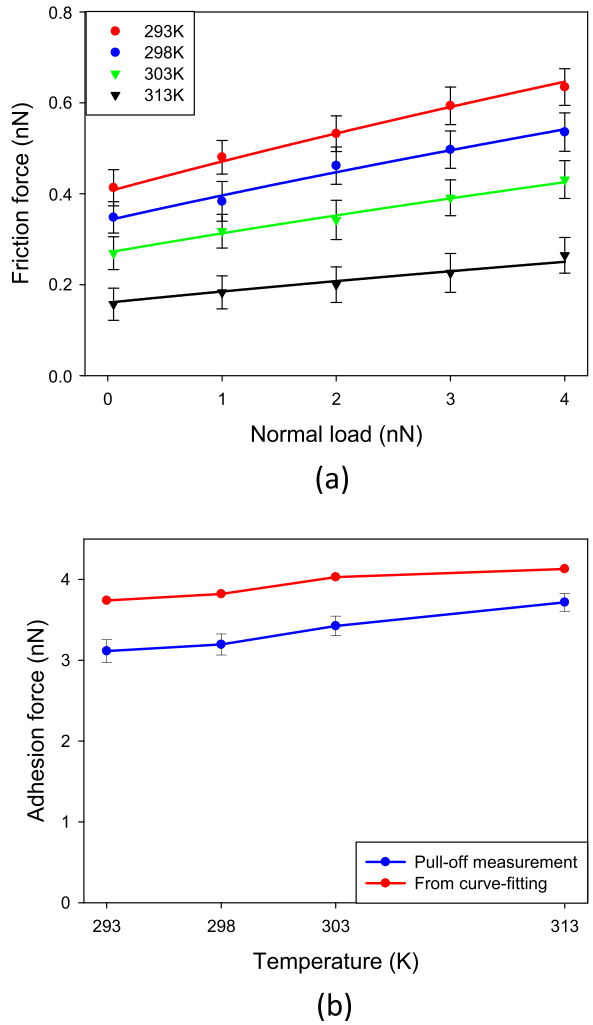

FIG. 2. Frictional Properties of 1L BNNS. (a) The dependence of the measured frictional force on the applied normal load at different temperatures (AFM tip scan rate 1000 nm/s). (b) The comparison of the adhesion force that was obtained from the direct pull-off measurements with the values obtained from curve fitting.

Figure 3(a) shows the measured frictional force on the 1L BNNS surface as a function of the AFM tip scan rate under the same applied load of 1 nN at different sample temperatures. The data show that a modest increase in the sample temperature results in a substantially lower frictional force. Figure 3(b) shows the dependence of the frictional force on the AFM scan rate for BNNSs of various thicknesses at the same sample temperature of 293 K. The frictional force is found to increase with the AFM tip scan rate and decrease with an increase of the sample thickness, both of which are consistent with prior reports in the literature for graphene.[9,25] A higher AFM tip scan rate tends to increase the frictional force through the puckering deformation of the sheet in contact.[25,26] The puckering effect originates from the out-of-plane deformation of the underlying sheet caused by the pushing of an AFM tip, which in turn resists the sliding of the AFM tip. The puckering effect is more pronounced in thinner sheets that possess lower bending rigidities. Under the same testing conditions, Figure 3(b) shows that the 1L BNNS consistently possesses a higher frictional force than the examined few-layer BNNSs. The dependence of the frictional force on the AFM tip scan rate (V) can be well-fitted using a logarithmic relationship that is given as[9,27,28]

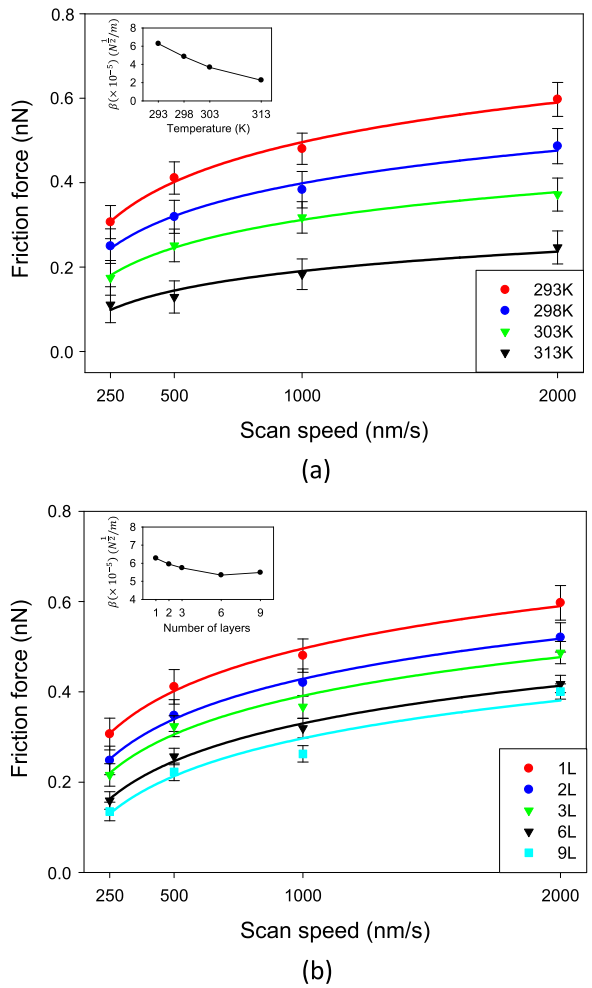

FIG. 3. The dependence of the frictional force on the AFM tip scan rate. All measurements were performed with a normal load of 1 nN. (a) 1L BNNS. (b) Mono- and multi-layer BNNSs at 293 K. The solid lines are the respective fitting curves to the experimental data sets (dots), and the inset plots show the respective values of β obtained from curve fitting.

$$f = f^* - \left(\beta k_B T \log\left(\frac{V_0}{V}\right)\right)^{\frac{2}{3}}, \quad (1)$$

where k_B is the Boltzmann constant, T is the temperature, f^* is the maximum frictional force before jumping in the stick-slip model, V_0 is the critical velocity above which the frictional force tends to be unchanged, and β is the parameter that depends on the shape of the energy landscape. For the tested AFM scan rates (250–2000 nm/s), the value of β for the examined 1L BNNS is found to be within the range of 2.3×10^5–6.3×10^5 $N^{1/2}$/m through curve fitting with an assumed V_0 of 2300 nm/s and is displayed as an inset plot in Figure 3(a). The data show a decreasing trend of β with the sample temperature. The influence of the sample temperature on the frictional force can be ascribed to the fact that a higher sample temperature results in a smaller surface roughness as shown in Figure S2 (supplementary material) and thus a smaller frictional force. It is worth mentioning here that an increase in the sample temperature results in a slight increase of the tip-sample adhesion force (Figure S3 of the supplementary material). Our results suggest that the surface roughness plays a more influential role in governing the frictional properties of BNNS than the AFM tip-sample adhesion force, which is supported by the data shown in Figure 3(b) that the thicker BNNS possesses lower frictional force. The observed lower frictional force for the thicker BNNS can be ascribed to the fact that the surface roughness is smaller for the thicker BNNS and the topographically smoother surface results in a lower friction force. It is noted that the adhesion force at the same sample temperature is of small variations for BNNSs of various thicknesses as displayed in Figure S3 (supplementary material) and is unlikely to be the major factor that accounts for the observed decreasing trend of the frictional force for thicker BNNS. The inset plot in Figure 3(b) shows the values of β that were obtained from curve-fitting of the displayed data sets shown in Figure 3(b). It is noticed that the value of β exhibits a decreasing trend with the BNNS sample thickness and tends to flatten out for the BNNS of six or more layers.

The data shown in Figures 2 and 3 reveal that a modest increase of the sample temperature by 5 or 10 K results in a sizeable drop of the frictional force. The observed frictional force decrease can be ascribed to the fact that thermal excitations at a higher temperature provide more energy to overcome the local energy barrier and enable slips. It is suggested that kinetic friction force has an exponential dependence on the sample temperature (T) that is given as[7]

$$f \propto \exp(U/k_B T), \quad (2)$$

where U is the activation energy of the contact rupture. Therefore, the activation energy U can be obtained through curve-fitting the temperature-dependent measurements. Figure 4(a) shows the dependence of the friction force on the sample temperature for all the examined BNNSs on an inverse temperature ($1/T$) scale, which can be well-fitted by using Eq. (2). Based on the frictional force data for the examined mono- and few-layer BNNS samples, the activation energy U is found to be about 0.354 ± 0.007 eV and is displayed in Figure 4(b). The calculated activation energy

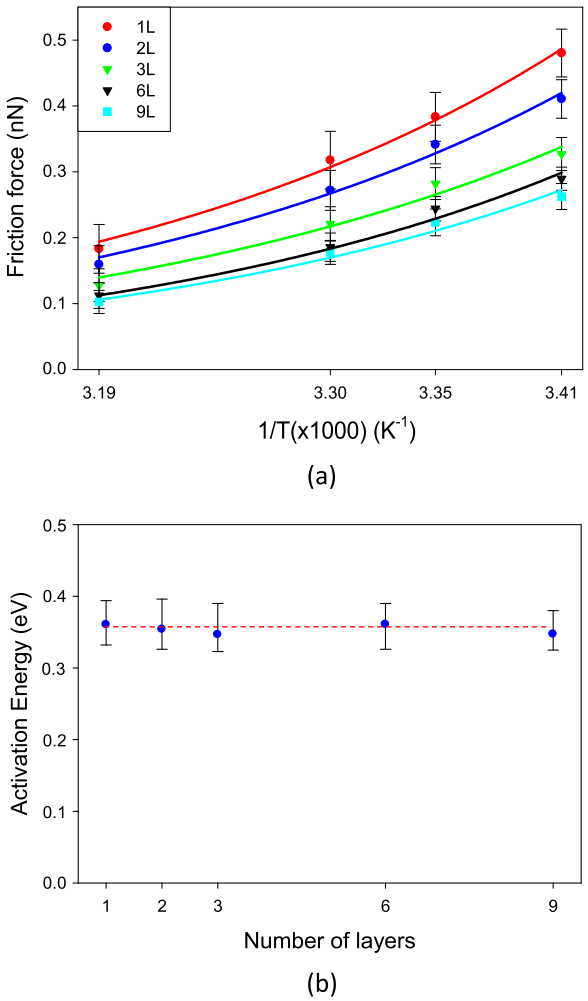

FIG. 4. (a) The effect of the sample temperature on the frictional force for mono- and multi-layer BNNSs (x-axis: temperature inverse). All measurements were performed with a normal load of 1 nN and an AFM scan rate of 1000 nm/s. The solid lines are the respective fitting curves based on the exponential relationship given by Eq. (2). (b) The calculated BNNS activation energy. The dashed line indicates the average value.

values stay in a narrow range and display a rather independent trend with respect to the sample thickness.

Prior research reports values of ~0.1 eV for the activation energy of graphene or graphite,[10,29] which is substantially lower than the value for h-BN sheets reported in this work. The high energy barrier observed for the h-BN surface as compared with graphene can be explained from their difference in bond structures. The hexagonal BN lattice is composed of alternatively positioned boron and nitrogen atoms. Due to their difference in size, the BN lattice network is topographically corrugated as compared with the smooth surface of graphene. Furthermore, B-N bonds in h-BN sheets are partially ionic in nature. The polarized electronic structure induces unsymmetrical partial charge distribution on the h-BN surface,[30] which leads to electrostatic interactions with non-charged contact bodies through dipole-induced dipole interactions. Therefore, it is energetically favorable to scan an electrically neutral graphene surface as compared with an electronically corrugated h-BN surface.[31]

The polarized electronic structure of B-N bonds in h-BN also influences its overall structural configuration, in particular, its surface roughness. Thin h-BN sheets reportedly possess

a negative in-plane thermal expansion coefficient,[32] as compared with the positive thermal expansion coefficient of the silicon oxide substrate. This implies that the h-BN sheet would shrink at a higher temperature, which results in more pronounced ripple effects and a higher surface roughness. The measured decreasing trend of the surface roughness with the sample temperature indicates that the h-BN sheet was actually under tension instead of compression when the temperature increased. This counterintuitive observation is probably caused by the strong interlayer binding interaction in h-BN sheets[33] as well as the strong interfacial binding interaction between the bottom layer of the h-BN sheet and the substrate.[20] The thermal expansion of the substrate as a result of temperature increases induces an in-plane stretching force to the bottom layer of the h-BN sheet and the whole h-BN sheet is stretched through the interlayer binding interactions, which in turn leads to a smoother surface and a lower surface roughness.

The energy landscape of the h-BN surface possesses a spatial periodicity. The energy barrier width can be estimated from the measured the dependence of the frictional force on the scan velocity. Here, the energy landscape is assumed to follow a sinusoidal shape, and then the energy barrier width, a, is given as $a = \frac{3\pi}{2\sqrt{2}}\frac{\sqrt{f^*}}{\beta}$.[27] Based on the data shown in Figure 3(b), a is found to be within a narrow range of 1.3 Å–1.4 Å for 1L–9L BNNSs, which indicates that the energy barrier width is independent of the BNNS thickness.

In summary, the temperature-dependent frictional properties of mono- and few-layer h-BN sheets were characterized by using AFM techniques. The measurements reveal that the frictional force on ultra-thin h-BN sheets is quite sensitive to temperature variation. The activation energy of the contact rupture for the examined BNNSs is found to be substantially higher than the reported values for graphene, which is attributed to the corrugated topographic and electronic structures in h-BN as compared with smooth and electrically neutral surfaces in graphene. This work is useful to better understand the physical properties of h-BN materials and in the pursuit of their applications, in particular, as substrate materials in nano electronic devices.

See supplementary material for the details about the Raman spectra and the surface roughness of mono- and few-layer BNNS flakes and the adhesion force between AFM tips and BNNS flakes.

This work was supported by U.S. Air Force Office of Scientific Research—Low Density Materials program under Grant No. FA9550-15-1-0491 and by National Science Foundation under Grant No. CMMI-1429176.

[1]A. Bosak, J. Serrano, M. Krisch, K. Watanabe, T. Taniguchi, and H. Kanda, Phys. Rev. B **73**, 041402 (2006).
[2]L. Boldrin, F. Scarpa, R. Chowdhury, and S. Adhikari, Nanotechnology **22**, 505702 (2011).
[3]T. Ouyang, Y. Chen, Y. Xie, K. Yang, Z. Bao, and J. Zhong, Nanotechnology **21**, 245701 (2010).
[4]L. H. Li, J. Cervenka, K. Watanabe, T. Taniguchi, and Y. Chen, ACS Nano **8**, 1457 (2014).
[5]G. Cassabois, P. Valvin, and B. Gil, Nat. Photonics **10**, 262 (2016).
[6]C. R. Dean, A. F. Young, I. Meric, C. Lee, L. Wang, S. Sorgenfrei, K. Watanabe, T. Taniguchi, P. Kim, K. L. Shepard, and J. Hone, Nat. Nanotechnol. **5**, 722 (2010).
[7]I. Barel, M. Urbakh, L. Jansen, and A. Schirmeisen, Phys. Rev. Lett. **104**, 066104 (2010).
[8]P. Hänggi, P. Talkner, and M. Borkovec, Rev. Mod. Phys. **62**, 251 (1990).
[9]L. Jansen, H. Hölscher, H. Fuchs, and A. Schirmeisen, Phys. Rev. Lett. **104**, 256101 (2010).
[10]X. Zhao, M. Hamilton, W. G. Sawyer, and S. S. Perry, Tribol. Lett. **27**, 113 (2007).
[11]A. Smolyanitsky, RSC Adv. **5**, 29179 (2015).
[12]C. M. Mate, G. M. McClelland, R. Erlandsson, and S. Chiang, Phys. Rev. Lett. **59**, 1942 (1987).
[13]H. Hölscher, U. D. Schwarz, and R. Wiesendanger, Europhys. Lett. **36**, 19 (1996).
[14]H. Hölscher, A. Schirmeisen, and U. D. Schwarz, Philos. Trans. R. Soc., A **366**, 1383 (2008).
[15]M. Urbakh, J. Klafter, D. Gourdon, and J. Israelachvili, Nature **430**, 525 (2004).
[16]R. V. Gorbachev, I. Riaz, R. R. Nair, R. Jalil, L. Britnell, B. D. Belle, E. W. Hill, K. S. Novoselov, K. Watanabe, T. Taniguchi, A. K. Geim, and P. Blake, Small **7**, 465 (2011).
[17]C. T. Gibson, G. S. Watson, and S. Myhra, Scanning **19**, 564 (1997).
[18]D. F. Ogletree, R. W. Carpick, and M. Salmeron, Rev. Sci. Instrum. **67**, 3298 (1996).
[19]Q. Cai, L. H. Li, Y. Yu, Y. Liu, S. Huang, Y. Chen, K. Watanabe, and T. Taniguchi, Phys. Chem. Chem. Phys. **17**, 7761 (2015).
[20]S. P. Koenig, N. G. Boddeti, M. L. Dunn, and J. S. Bunch, Nat. Nanotechnol. **6**, 543 (2011).
[21]W. Gao and R. Huang, J. Phys. Appl. Phys. **44**, 452001 (2011).
[22]T. Li and Z. Zhang, J. Phys. Appl. Phys. **43**, 075303 (2010).
[23]W. G. Cullen, M. Yamamoto, K. M. Burson, J. H. Chen, C. Jang, L. Li, M. S. Fuhrer, and E. D. Williams, Phys. Rev. Lett. **105**, 215504 (2010).
[24]X. Chen, M. Zheng, C. Park, and C. Ke, Appl. Phys. Lett. **102**, 121912 (2013).
[25]C. Lee, Q. Li, W. Kalb, X.-Z. Liu, H. Berger, R. W. Carpick, and J. Hone, Science **328**, 76 (2010).
[26]Y. Dong, X. Z. Liu, P. Egberts, Z. Ye, R. W. Carpick, and A. Martini, Tribol. Lett. **50**, 49 (2013).
[27]E. Riedo, E. Gnecco, R. Bennewitz, E. Meyer, and H. Brune, Phys. Rev. Lett. **91**, 084502 (2003).
[28]E. Riedo and E. Gnecco, Nanotechnology **15**, S288 (2004).
[29]A. Schirmeisen, L. Jansen, and H. Fuchs, Phys. Rev. B **71**, 245403 (2005).
[30]M. L. Cohen and A. Zettl, Phys. Today **63**(11), 34 (2010).
[31]G. Tocci, L. Joly, and A. Michaelides, Nano Lett. **14**, 6872 (2014).
[32]B. Yates, M. J. Overy, and O. Pirgon, Philos. Mag. **32**, 847 (1975).
[33]A. Niguès, A. Siria, P. Vincent, P. Poncharal, and L. Bocquet, Nat. Mater. **13**, 688 (2014).